Supporting information for "Self-Adjusted All-Dielectric Metasurface for Deep Ultraviolet Femtosecond Pulses Generation"

Sergey Makarov,[1] Anton Tsypkin,[1] Tatiana Voytova,[1] Valentin Milichko,[1]
Ivan Mukhin,[1,2] Alexey Yulin,[1] Sergey Putilin,[1] Mikhail Baranov,[1]
Alexander Krasnok,[1] Ivan Mozharov,[2] and Pavel Belov[1]
[1]*ITMO University, St. Petersburg 197101, Russia and*
[2]*St. Petersburg Academic University, St. Petersburg 194021, Russia*

I. FILM THICKNESS OPTIMIZATION

Optimization of surface nanostructuring is represented in Fig. S1. In all experiments, surface scanning by a focused laser beam with a repetition rate of 10 kHz and a scan speed of 20 μm/s provides $\approx$ 450 absorbed laser pulses per spot. The best quality of nanostructures was observed for d = 100 nm (Fig. S1). As it is discussed in the main text, this film thickness provides excitation of a planar waveguide mode at a wavelength of 800 nm. The interference maxima near the "point like" source give inhomogeneous electric field distribution. However, periodic interference pattern can be observed only around a thickness of 100 nm, whereas the other thicknesses do not demonstrate such effective energy conversion to the waveguide mode and the electromagnetic field enhancement up to 1.5 times. Numerical simulations are performed by using time-domain solver in the commercial software CST Microwave Studio. Refractive index of amorphous silicon is taken from Palik [1].

II. ANALYTICAL MODEL FOR LASER-INDUCED METASURFACE FORMATION

The most widely accepted theory of laser-induced periodical surface structures (LIPSS) is based on the interference of the incident laser beam with some form of a surface-scattered electromagnetic wave. The work of Sipe et al. [2] represents a first-principle theory which takes into consideration the interaction of an electromagnetic wave with a microscopically rough surface. This theory predicts possible LIPSS wave vectors k of the surface [with $|\mathbf{k}|=2\pi/\Lambda$] as a function of the laser parameters angle of incidence u, polarization direction, and wave vector of the incident radiation $\mathbf{k}_L$ (with $|\mathbf{k}_L|=2\pi/\lambda$) which has a component k_i in the surface plane (Fig. S2) and surface parameters (dielectric constant and surface roughness). It leads to an expression for the inhomogeneous energy deposition into the irradiated material which is proportional to $\eta(\mathbf{k},\ \mathbf{k}_i)\times|b|$, where η is a response function describing the efficacy with which the surface roughness at k leads to inhomogeneous absorption of radiation. The second factor b represents a measure of amplitude of the surface roughness at $\mathbf{k}$ which is a slowly varying function for a surface with a homogeneously distributed roughness. In contrast to the behavior of b, the efficacy factor η can exhibit sharp peaks at certain $\mathbf{k}$ values which then determine the spatial ripple periods. It worth noting that once the LIPSS are formed, the Fourier spectrum of the surface $b(\mathbf{k})$ can also exhibit sharp peaks coincident with the peaks in $\eta(\mathbf{k})$ which were initially responsible for the surface damage.

We briefly summarize the mathematical definitions needed to calculate the efficacy factor on the basis of the mentioned first-principle theory. It will use the general expressions given in that reference in order to get simplified equations for practical use in the present situation. In the theory of Sipe et al., the efficacy factor is defined as

$$\eta(\mathbf{k},\mathbf{k}_i) = 2\pi|\upsilon(\mathbf{k}_+) + \upsilon^*(\mathbf{k}_-)|. \tag{S1}$$

For the two cases of s- or p-polarized light, incident under an angle of θ and having polarization vectors and a wave vector component k_i, the complex function υ is given by

$$\upsilon(\mathbf{k}_\pm, s-pol.) = [h_{ss}(k_\pm)(\hat{\mathbf{k}}\pm\cdot\hat{\mathbf{y}})^2 + h_{kk}(k_\pm)(\hat{\mathbf{k}}\pm\cdot\hat{\mathbf{x}})^2]\gamma_t|t_s(k_i)|^2, \tag{S2}$$

or

$$\begin{aligned}\upsilon(\mathbf{k}_\pm, p-pol.) = [h_{ss}(k_\pm)(\hat{\mathbf{k}}_\pm\cdot\hat{\mathbf{x}})^2 + h_{kk}(k_\pm)\\ \times(\hat{\mathbf{k}}_\pm\cdot\hat{\mathbf{y}})^2]\gamma_t|t_s(k_i)|^2 + h_{kz}(k_\pm)\\ \times(\hat{\mathbf{k}}_\pm\cdot\hat{\mathbf{y}})\gamma_z\varepsilon t_x^*(\mathbf{k}_i)t_z(\mathbf{k}_i) + h_{zk}(k_\pm)\\ \times(\hat{\mathbf{k}}_\pm\cdot\hat{\mathbf{y}})\gamma_t t_x(\mathbf{k}_i)t_z^*(\mathbf{k}_i)\\ +h_{zz}(k_\pm)\gamma_z\varepsilon|t_z(\mathbf{k}_i|^2,\end{aligned} \tag{S3}$$

with the inner products

$$(\hat{\mathbf{k}}_\pm\cdot\hat{\mathbf{y}}) = (sin\theta\pm\kappa_y)/\kappa_\pm \tag{S4}$$

and

$$(\hat{\mathbf{k}}_\pm\cdot\hat{\mathbf{y}}) = \kappa_x/\kappa_\pm. \tag{S5}$$

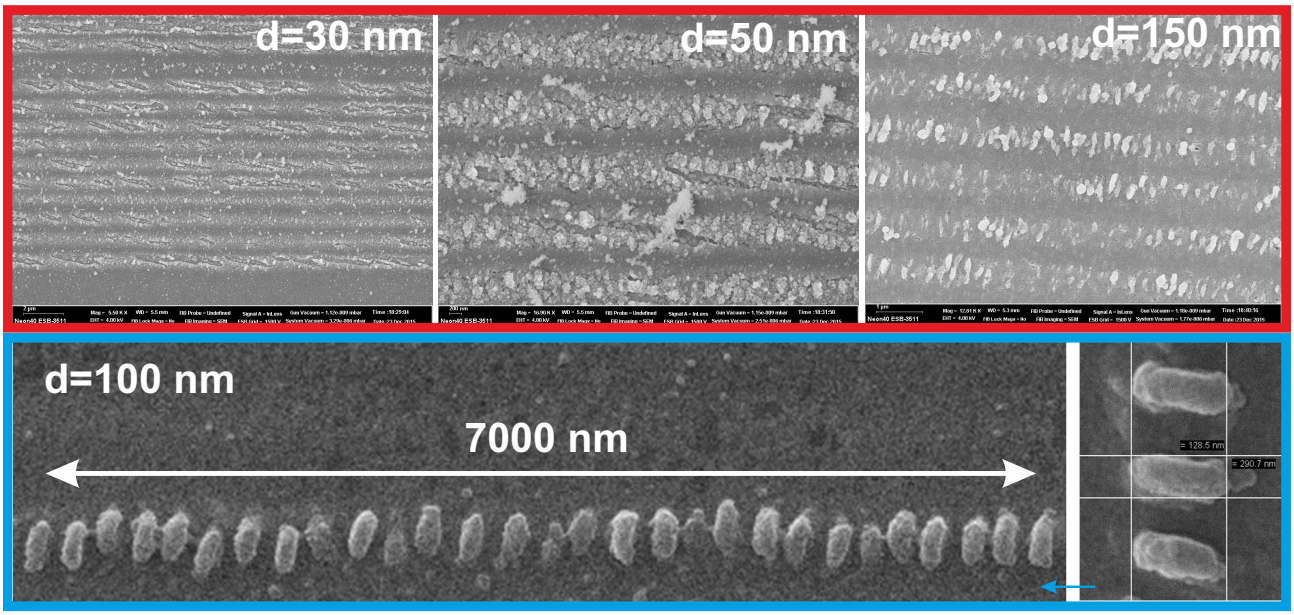

FIG. S1. SEM images of nanostructured films by femtosecond laser irradiation with different thicknesses d.

Here, the definition $\kappa_\pm = [\kappa_x^2 + (sin\theta \pm \kappa_y)^2]^{1/2}$ has been used and all lengths have been normalized with the factor $\lambda/(2\pi)$. Hence, the dimensionless LIPSS wave vectors $\kappa = k \cdot \lambda(2\pi) \equiv \lambda/\Lambda$ are used in the following. With these definitions and with ε being the complex dielectric function of the material at the irradiation wavelength, the functions h_{ss}, h_{kk}, h_{kz}, h_{zk}, and h_{zz} used in Eqs. (2) and (3) can be expressed as

$$h_{ss}(k_\pm) = \frac{2i}{\sqrt{1-\kappa_\pm^2} + \sqrt{\varepsilon - \kappa_\pm^2}}, \tag{S6}$$

$$h_{kk}(k_\pm) = \frac{2i\sqrt{(\varepsilon - \kappa_\pm^2)(1-\kappa_\pm^2)}}{\varepsilon\sqrt{1-\kappa_\pm^2} + \sqrt{\varepsilon - \kappa_\pm^2}}, \tag{S7}$$

$$h_{kz}(k_\pm) = \frac{2i\kappa_\pm\sqrt{\varepsilon - \kappa_\pm^2}}{\varepsilon\sqrt{1-\kappa_\pm^2} + \sqrt{\varepsilon - \kappa_\pm^2}}, \tag{S8}$$

$$h_{zk}(k_\pm) = \frac{2i\kappa_\pm\sqrt{1-\kappa_\pm^2}}{\varepsilon\sqrt{1-\kappa_\pm^2} + \sqrt{\varepsilon - \kappa_\pm^2}}, \tag{S9}$$

and

$$h_{zz}(k_\pm) = \frac{2i\kappa_\pm^2}{\varepsilon\sqrt{1-\kappa_\pm^2} + \sqrt{\varepsilon - \kappa_\pm^2}}. \tag{S10}$$

The complex functions t_s, t_x, and t_z are given by

$$t_s(\mathbf{k}_i) = \frac{2|cos\theta|}{|cos\theta| + \sqrt{\varepsilon - (sin\theta)^2}} \tag{S11}$$

$$t_x(\mathbf{k}_i) = \frac{2\sqrt{\varepsilon - (sin\theta)^2}}{\varepsilon|cos\theta| + \sqrt{\varepsilon - (sin\theta)^2}} \tag{S12}$$

and

$$t_z(\mathbf{k}_i) = \frac{2sin\theta}{\varepsilon|cos\theta| + \sqrt{\varepsilon - (sin\theta)^2}} \tag{S13}$$

The surface roughness is included in the theory in the factors γ_t and γ_z via two numerical factors, s (shape factor) and f (filling factor), by

$$\gamma_t = \frac{\varepsilon - 1}{4\pi(1 + 0.5(1-f)(\varepsilon-1)(F(s) - R \cdot G(s))} \tag{S14}$$

and

$$\gamma_z = \frac{\varepsilon - 1}{4\pi(\varepsilon - (1-f)(\varepsilon-1)(F(s) + R \cdot G(s))} \tag{S15}$$

with R=(ε-1)/(ε+1) and the scalar functions

$$F(s) = \sqrt{s^2+1} - s, \tag{S16}$$

and

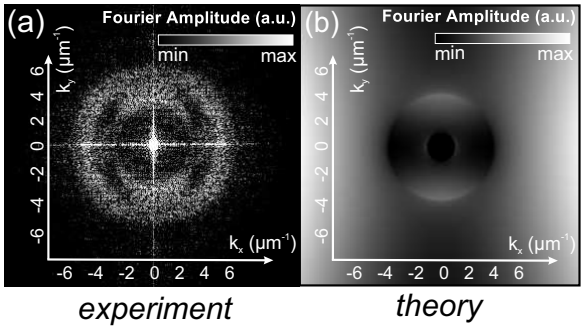

FIG. S2. Experimental (a) and theoretical (b) spatial 2D Fourier spectra of the fabricated metasurface.

$$Q(s) = 0.5(\sqrt{s^2+4}+s) - \sqrt{s^2+1}. \qquad \text{(S17)}$$

Following Ref. [2], the surface roughness was modeled with the values s=0.4 and f =0.1, which represent the assumption of spherically shaped islands.

On the basis of Eqs. (S1)–(S17) it is possible to calculate numerically the efficacy factor h as a function of the normalized LIPSS wave vector components κ_x, κ_y at given values for the irradiation parameters (θ, λ, and polarization direction) and for parameters characterizing the optical (ε) and the surface roughness properties (s and f).

In the case of bulk material with known complex refractive index ($n+i\cdot K$) and slightly rough surface, the resulting intensity distribution in a sub-surface layer can be characterized by a so-called "efficacy factor" $\xi(\vec{k}\,;\vec{k}_i)$, where $\vec{k}$ and $\vec{k}_i$ are the wave vectors of the resulting intensity distribution and incident light, respectively [2].

The calculated 2D Fourier spectrum of laser energy deposition (for n=3.90 and K=0.11 at λ=800 nm [1], see Section 1 of Supplementary Materials for details) exhibits pronounced maxima for structures with period around $\lambda/n \approx 205$ nm and with wavevectors perpendicular to the laser polarisation (Fig. S2b).

It is worth noting, that the surface plasmon-polaritons excitation [3–5] is unlikely to be the origin of the metasurface formation in our case, because the wavevector of the periodical arrays is perpendicular to polarization of the incident light (Fig. S2a), whereas plasmon-polaritons are mostly longitudinal waves [6]. Moreover, quality of nanostructuring is the best for 100-nm film as compared to the other a-Si:H films, revealing an important role of the waveguiding mode.

III. SPECTRAL AND SPATIAL CHARACTERIZATION OF LASER BEAMS

Spectrum of incident femtosecond laser pulses with a central wavelength of 800 nm is shown in Fig. S3a and has a width at half-maximum around 28 nm. We do not observed THG from our silica substrates, which have relatively low efficiency for direct THG [7] and much higher efficiencies in four-wave mixing schemes [8]. In the case of efficient generation of TH from the self-adjusted metasurface, we observed some changes in spatial distribution of the generated pulses. As shown in Fig. S3, the spatial distribution of the TH beam undergoes broadening and slight distortion. The measurements of the intensity distributions were carried out by means of laser beam profiler (Newport).

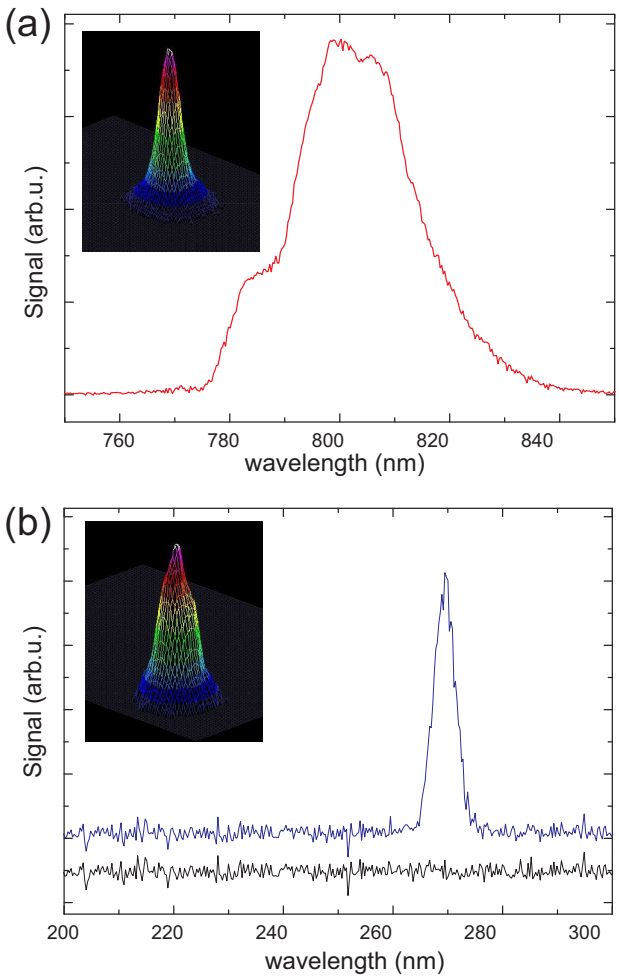

FIG. S3. (a) Spectrum of an incident femtosecond laser pulse and its spatial distribution. (b) Spectra of emission signal around third harmonic wavelength for a blank silica substrate (black curve) and for a self-adjusted metasurface (blue curve) and its spatial distribution.

IV. THIRD HARMONICS GENERATION FROM NONRESONANT NANOSTRUCTURE

In order to study of third harmonics generation from nonresonant surface nanostructure, we provided dense surface structuring in *single-shot regimes*, where each pulse damages an area of about 0.5×0.3 μm (Fig. S4a). Reflection spectrum of such structure does not contain any features at $\lambda = 800$ nm (Fig. S4b). Measured UV signal at the maximum intensity 80 GW/cm^2 reveals 2-fold decrease as compared to UV signal from smooth silicon film with the same thickness.

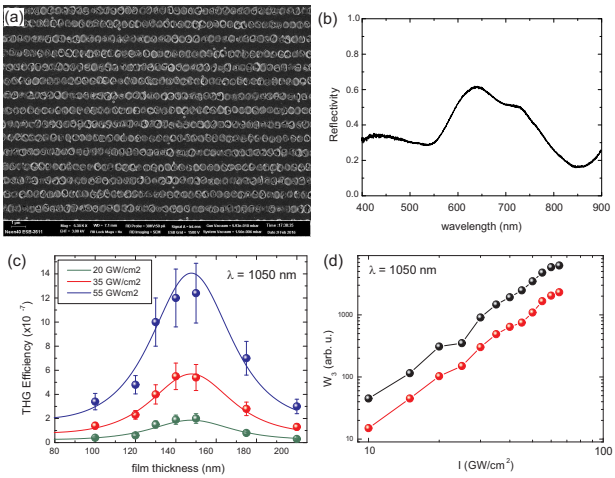

FIG. S4. (a) SEM image of nonresonant surface nanostructure. (b) Reflection spectrum of the nonresonant surface nanostructure. (c) Experimental (circles) and theoretical (lines) dependencies of third harmonic generation (THG) efficiency on Si film thickness at various pump intensities: 20 GW/cm^2 (black), 35 GW/cm^2 (red), 55 GW/cm^2 (blue) of 1050-nm fs-laser. (d) Experimental dependencies of third harmonic signal generated by 1050-nm pulses from initial (black dots) and nanostructured Si films with 100-nm thickness on fused silica substrate with resonant geometry for 800-nm.

Additionally, we observed the dependence of THG efficiency on orientation of polarization of pump laser. When the laser pulses irradiate the self-adjusted metasurface, the TH signal generated by the beam with polarization parallel to rows of the metasurface is 2.1 times higher than for the beam with perpendicular polarization.

Nonresonant regime was additionally tested as following. We fabricate self-adjusted metasurface under 800-nm laser irradiation, and then generate TH signal by using 1050-nm laser pulses and compare it with TH signal from smooth a-Si:H film at the same wavelength. Similarly to the experiments at 800 nm, we initially found the most resonant film thickness, which turned out to be 150 nm (Fig. S4c). For this experiment, we employed Yb^{+3} laser (TeMa, "Avesta Project Ltd.") emitting pulses with central wavelength 1050 nm, spectral width 7 nm, and duration 150 fs. The THG dependencies on film thicknesses at different intensities correlate with the results of our analytical model (see Section VI) for the following parameters: $\chi^{(3)} = 1.2 \cdot 10^{-18} m^2/V^2$, n(Si,$\lambda$ = 350nm) = 5.44+i·2.997, n(Si,λ = 1050nm) = 3.556+i·0, n(SiO_2,λ = 350nm) = 1.477+i·0, n(SiO_2,λ = 1050 nm)=1.45+i·0. This experiment proofs the importance of Fabry-Perot resonances for IR pulses as well as for 800 nm. Further step is to study THG under 1050-nm irradiation from the metasurface, which is resonant only for 800 nm. The result of these measurements are shown in Fig. S4d, where 3-fold average decrease of TH signal was observed in broad range of intensities.

The measurements of THG in non-resonant regimes support the idea, that TH enhancement observed for self-adjusted metasurfaces is caused by specific periodicity of the structure rather than roughness with larger effective surface area.

V. ESTIMATION OF UV PULSE DURATION

The spreading of the pump pulse can be estimated as follows. The finite thickness of the Si film will contribute to the temporal broadening of the input pulse and the estimate is $T = GVD \cdot d/\tau$ where d is the thickness of the film and τ is the duration of the input pulse. For GVD of silicon at 800 nm this gives the value of subfemtoseconds and thus it can be neglected even if we take into account that the reflection at the interfaces increases the effective optical thickness of the film by a factor of five (the highest Q of the system).

The resonant localized mode also causes the increase of the duration of the pump signal. This contribution can be estimated as the dissipation time of the filed in the resonator and for the quality factor $Q = 5$ at the wavelength 800 nm it is $\approx$ 15 fs which is smaller but comparable with the duration of our input pulse. More exact estimate obtained from the solution of the oscillator equation with $Q = 5$ excited by 40 fs pulse of Gaussian shape gives the lifetime of the mode at the fundamental frequency to be less than 50 fs. So the pulse of the third harmonic is expected to have the duration less then 30 fs.

VI. MODEL FOR THIRD HARMONICS GENERATION

Let us consider a one-dimensional system consisting of silicon film with thikness d placed on the silica substrate and air at the another side. We assume that the system is pumped by the incident radiation from the substrate side at normal incidence as it shown in Fig. S5. The silicon film has a cubic nonlinearity and therefore the incident

wave causes the emission of the radiation at the triple frequency.

We assume that the third harmonic is much weaker compared to the fundamental one. This assumption is fulfilled for the experimental conditions - the intensity of the third harmonic is less than 10^{-6} of the intensity of the fundamenatl harmonic. This assumption allows us to split the theoretical problem in two parts and solve them separately. The first part of the problem is to calculate the spatial distribution of the field of the fundamental harmonics neglecting the effect of the third and higher harmonics on the fundamental one. Knowing the nonlinearity and the distribution of the fundamental harmonic field it is possible to find the distribution of the nonlinear current at the frequency of the third harmonic. The last step is to solve the problem of the emission of the electromagnetic waves by the nonlinear current.

To solve these problems we use well known transfer matrix method [9]. Let us denote the air by index $j = 1$, fused silica substrate by index $j = 2$ and silicon by index $j = 3$, so $k_j = \omega n_j/c$ is the wavevector in the medium with index j, n_j is the refractive index, c is the speed of light. Fresnel coefficients for the transmission and reflection, respectively, will be expressed as $r_{ij} = (n_i - n_j)/(n_i + n_j)$, $t_{ij} = 2n_i/(n_i + n_j)$. The system is pumped by incident radiation with field strength E_0 at the first harmonic frequency ω_1. The procedure of the calculation of the field is standard but it is long and thus we do not discuss it here in detail giving only the final expression. The transmitted first harmonic field strenght $E_t(\omega_1)$ is determined by the transmission coefficient $T(\omega_1)$ as:

$$E_t(\omega_1) = T(\omega_1)E_0 = \\ = \frac{t_{31}(\omega_1)t_{23}(\omega_1)t_{12}(\omega)e^{ik_1(\omega_1)z}}{e^{ik_3(\omega_1)d} + r_{13}(\omega_1)r_{32}(\omega_1)e^{-ik_3(\omega_1)d}}E_0. \quad \text{(S18)}$$

The fundumental field at the location of nonlinear layer $(0 < z' < d)$ is determined by the expression:

$$E_{z'}(\omega_1) = f_1(\omega_1, z')E_0 = \\ = \frac{t_{23}(\omega_1)t_{12}(\omega_1)\left(e^{ik_3(\omega_1)z'} - r_{13}(\omega_1)e^{-ik_3(\omega_1)z'}\right)}{e^{ik_3(\omega_1)d} + r_{13}(\omega_1)r_{32}(\omega_1)e^{-ik_3(\omega_1)d}}E_0. \quad \text{(S19)}$$

The denominator in the expression for $f_1(\omega_1, z')$ can become small at the resonances and this means the increase of the intensity of the fundamental harmonics at resonant frequencies. We calculate the nonlinear current at third harmonic frequency $\omega_3 = 3\omega_1$ assuming that the current is co-directed with the electric field of the fundamental mode and the nonlinear coefficient does not depend on the frequency $j_n(\omega_3, z') = i\omega_3\epsilon_0\chi^{(3)} \cdot E_{z'}(\omega_1)^3$. An important fact is that the intensity of the light at the fundamental harmonics is not spatially uniform in the film but has pronounced maxima so that the nonlinear current has pronounced maxima too. That is why some parts of the structure contribute to the third harmonic generation more then the others.

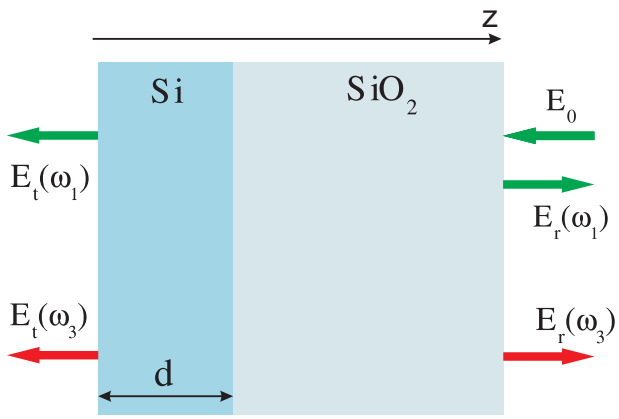

FIG. S5. Geometry of the problem of third harmonic generation from the silicon film placed on the fused silica substrate

The next step is the calculation of the waves excited by the nonlinear current. This can conveniently done using Green functions formalism. We can express the amplitude of the emitted third harmonic $E(\omega_3)$ through the integral of the product of the Green function and the nonlinear current. The third harmonic field on the left of the film (in the air) $E_t(\omega_3)$ given by:

$$E_t(\omega_3) = -\int_0^d G(z, z')j_n(\omega_3, z')dz', \quad \text{(S20)}$$

$$G(z, z') = \frac{t_{31}(\omega_3)e^{ik_1(\omega_3)z}}{2i\epsilon_0\omega_3} \times \\ \times \frac{e^{ik_3(\omega_3)(d-z')} + r_{32}(\omega_3)e^{-ik_3(\omega_3)(d-z')}}{e^{ik_3(\omega_3)d} + r_{13}(\omega_3)r_{32}(\omega_3)e^{-ik_3(\omega_3)d}}. \quad \text{(S21)}$$

From the expression (S20) it is clearly seen that the efficiency of the third harmonics depends not only on the intensity distribution of the nonlinear current but also on the structure of the Green function. Thus the resonances on the frequency of the third harmonics can also enhance the emission of the radiation. The later is known as Purcell effect in quantum optics. However for the experimental conditions the losses are high at the frequency of the third harmonic and thus only the radiation from a thin layer close to the interface is important.

Finally to estimate the efficiency of the third harmonic generation we introduce the coefficient showing the ratio of the energy flow W in the third harmonic in the air to the energy flow in the transmitted fundamental wave:

$$\eta = \frac{W_3}{W_1} = \frac{|E_t(\omega_3)|^2}{|E_t(\omega_1)|^2} \quad \text{(S22)}$$

Now we can calculate the radiation efficiency for the experimental parameters. The parameter of nonlinear

susceptibility in our calculation is taken to be equal to $\chi^{(3)} = 1.2 \cdot 10^{-18} m^2/V^2$ [10, 11]. Our estimates show that the maximum of the third-harmonic generation efficiency is expected for 106-nm film and is equal to $\eta_{teor} = 8 \cdot 10^{-7}$. This estimate matches well to the experimentally measured efficiency reaching maximum value of $\eta_{exp} = 4.8 \cdot 10^{-7}$ for 100-nm Si-film. The theoretical and experimental dependencies of the generation efficiency on the thickness of the film is shown in panel (a) of Fig. 4.

[1] E. D. Palik, *Handbook of optical constants of solids* (Academic press, 1998).

[2] J. Sipe, J. F. Young, J. Preston, and H. Van Driel, Physical Review B **27**, 1141 (1983).

[3] J. Bonse, A. Rosenfeld, and J. Krüger, Journal of Applied Physics **106**, 104910 (2009).

[4] M. Huang, F. Zhao, Y. Cheng, N. Xu, and Z. Xu, Acs Nano **3**, 4062 (2009).

[5] A. Kuchmizhak, A. Ionin, S. Kudryashov, S. Makarov, A. Rudenko, Y. N. Kulchin, O. Vitrik, and T. Efimov, Optics letters **40**, 1687 (2015).

[6] H. Raether, *Surface plasmons on smooth surfaces* (Springer, 1988).

[7] T. Y. Tsang, Physical Review A **52**, 4116 (1995).

[8] R. Weigand and H. M. Crespo, Applied Physics B **111**, 559 (2013).

[9] D. Bethune, JOSA B **6**, 910 (1989).

[10] D. Moss, H. Van Driel, and J. Sipe, Applied physics letters **48**, 1150 (1986).

[11] D. Moss, E. Ghahramani, J. Sipe, and H. Van Driel, Physical Review B **41**, 1542 (1990).